Plasma-Treated Thickness-Controlled Two-Dimensional Black Phosphorus and Its Electronic Transport Properties

Jingyuan Jia,[†,‡] Sung Kyu Jang,[†,‡] Shen Lai,[†,‡] Jiao Xu,[†,‡] Young Jin Choi,[§] Jin-Hong Park,[*,∥] and Sungjoo Lee[*,†,‡,∥]

[†]SKKU Advanced Institute of Nanotechnology (SAINT), [‡]Center for Human Interface Nanotechnology (HINT), Samsung-SKKU Graphene Center, and [∥]College of Information and Communication Engineering, Sungkyunkwan University (SKKU), Suwon 440-746, Korea and [§]Department of NanoTechnology and Advanced Materials Engineering, Sejong University, Seoul 143-747, Korea

ABSTRACT We report the preparation of thickness-controlled few-layer black phosphorus (BP) films through the modulated plasma treatment of BP flakes. Not only does the plasma treatment control the thickness of the BP film, it also removes the chemical degradation of the exposed oxidized BP surface, which results in enhanced field-effect transistor (FET) performance. Our fabricated BP FETs were passivated with poly(methyl methacrylate) (PMMA) immediately after the plasma etching process. With these techniques, a high field-effect mobility was achieved, 1150 $cm^2/(V\ s)$, with an I_{on}/I_{off} ratio of $\sim 10^5$ at room temperature. Furthermore, a fabricated FET with plasma-treated few-layer BP that was passivated with PMMA was found to retain its $I-V$ characteristics and thus to exhibit excellent environmental stability over several weeks.

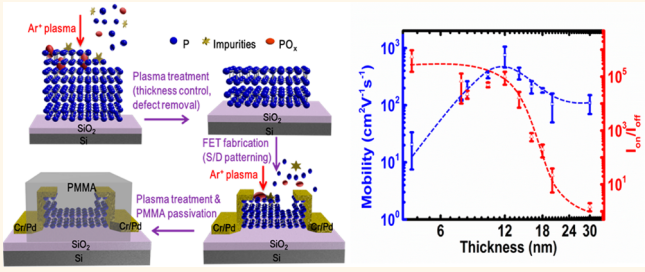

KEYWORDS: black phosphorus · 2-D material · plasma etching · 2-D thickness control · environmental stability

Two-dimensional crystals have attracted significant attention since the rise in popularity of graphene. However, graphene lacks a band gap,[1,2] so a two-dimensional gapped material with high mobility is highly sought.[3−5] Black phosphorus (BP) has been studied for decades and is known as a most stable allotrope of phosphorus with its unique orthorhombic structure.[6−8] Recent studies have shown that BP is an elemental layered material, with strong in-plane bonds and a weak van der Waals interlayer interaction that make it possible to obtain layered structures through mechanical cleavage.[3,4,8−11] The energy band gap of BP is reported to be 0.33 eV in the bulk and 1.8 eV for a monolayer,[4,9,11−13] and unlike transition metal dichalcogenides (TMD) such as MoS_2 and WSe_2, the energy band gap of BP retains its direct band gap character when the layer thickness varies.[5,9,11−14] Moreover, the carrier mobility of BP can theoretically be as high as 20000 $cm^2/(V\ s)$.[9] These fascinating properties mean that layer-structured BP is a promising semiconducting channel material for future nanoscale electronic devices and suitable for near and mid-infrared region optoelectronic device applications. However, there are several technological obstacles that must be overcome to enable the actual implementation and integration of BP devices. Although BP is known to be the most stable phosphorus allotrope,[6−8,15,16] recent experiments have demonstrated that after exposure to ambient conditions, BP exfoliated from the bulk is not environmentally stable because it reacts with oxygen and water molecules and forms a rough surface containing impurities,[17−24] which act as charge trapping centers and carrier scattering centers. As a result, considerable degradation of transistor performances, including decreases in mobility and threshold voltage shifts have been observed.[20−22] A theoretical study has also indicated that the surface of BP is hydrophilic due to its strong out of plane dipole moment.[9,20] In addition, the mechanical cleavage with tape of BP from the bulk is not as easily realized as for graphene and TMD materials, in that it

* Address correspondence to jhpark9@gmail.com, leesj@skku.edu.

Received for review January 7, 2015 and accepted August 22, 2015.

Published online August 24, 2015
10.1021/acsnano.5b04265

© 2015 American Chemical Society

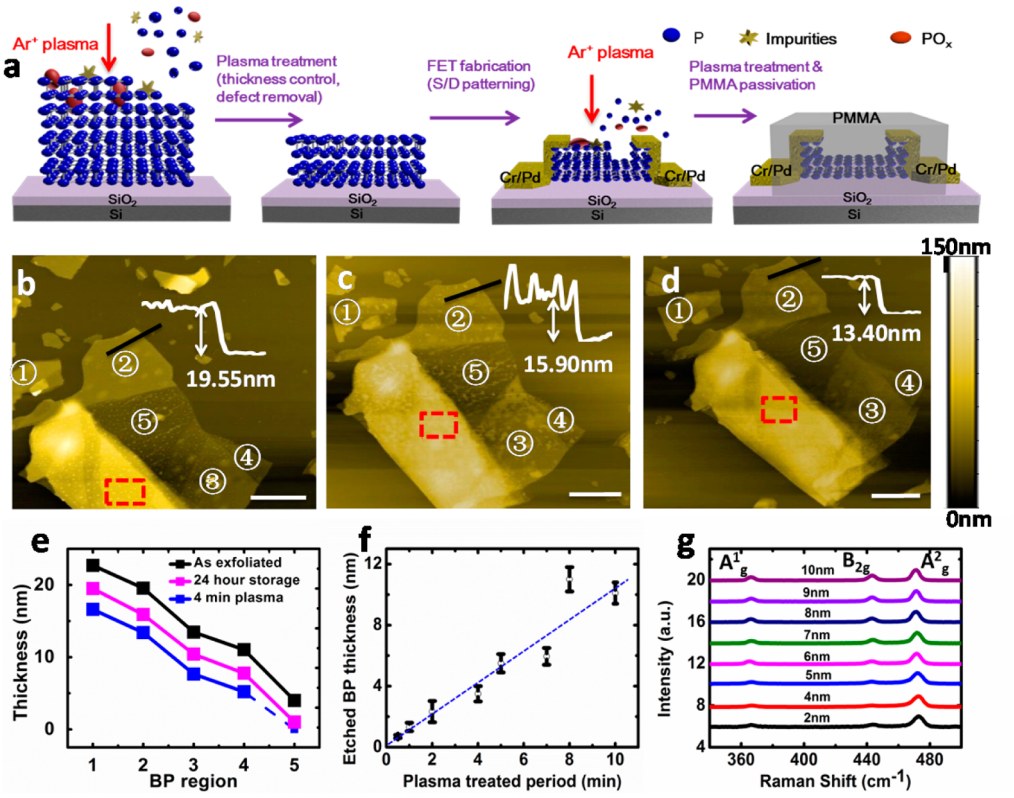

Figure 1. (a) Schematic diagram of the effects of the plasma treatment of a BP flake: thickness control, surface defect removal, and device fabrication process. AFM mapping images of a BP flake: (b) as-exfoliated, (c) after 24 h of storage, and (d) after plasma treatment for 4 min (scale bars: 2 μm); (e) BP thicknesses in regions ①–⑤ in panels b, c, and d; (f) etched BP thickness as a function of the duration of the plasma treatment; (g) Raman spectra of BP films with various thicknesses.

is difficult to control the layer thickness of the exfoliated film.[9]

In an attempt to resolve these two issues, we tested in this study a plasma etching process in which the thickness of the layered BP film can be controlled by modulating the plasma etching time. During this plasma etching process, the defects formed on the top surface of the exfoliated BP are removed. Our atomic force microscopy (AFM), scanning electron microscopy (SEM) and X-ray photoelectron spectroscopy (XPS) results show that the oxidants formed on the BP surface are removed by the plasma etching process, which results in a smooth surface morphology. It was also shown that thickness-controlled BP maintains excellent crystallinity after plasma etching, which was confirmed with Raman spectroscopy and high-resolution transmission electron microscopy (TEM). By using this method and the passivation of the fabricated BP field-effect transistors (FETs) with poly(methyl methacrylate) (PMMA), we achieved a hole mobility of 1150 $cm^2/(V\ s)$ and an I_{on}/I_{off} ratio of 10^5 at room temperature. These BP FETs also retain their $I-V$ characteristics over several weeks.

RESULTS AND DISCUSSION

Few-layer BP films were obtained by cleaving bulk BP crystals with blue Nitto tape, followed by Ar+ plasma treatment of various durations to achieve thickness-controlled BP films. Figure 1a shows a schematic illustration of the plasma treatment BP layer thinning process and the resulting removal of the impurities on the top surface of a BP film. The morphologies and thicknesses of the BP layers were examined by performing optical microscopy (OM), SEM, and AFM. After examination of the BP flakes with OM, the exfoliated BP samples were transferred onto Si substrates covered with thermally grown 285 nm SiO_2 layers for further characterization and for fabrication of back-gated BP FETs. As shown in Figure 1a, after patterning of source/drain electrodes, the exposed BP films are plasma-treated and passivated with PMMA. To find an optimal plasma treatment condition with which the BP thickness can be controlled by varying the plasma treatment duration without inducing damages on the morphology and crystal structure of the BP films, we examined various plasma power conditions at fixed pressure of 30 mTorr for 5 min. As can be seen in Figure S9, in the case of the plasma power below 350 W, no significant OM contrast changes were observed after plasma treatments. After plasma treatment at 400 W, the OM contrast changed too much and the surface became rough. Moderate OM contrast change was observed after the plasma treatments at 350 W. Further fine-tuning of plasma power was examined by

monitoring the etched BP surface with AFM mapping. Figure S10 shows the AFM mapping images of the BP films after plasma treatments at 325, 350, and 375 W, respectively. Considering uniform etching result on BP films and damages induced on the BP surface, the plasma treatment at 350 W was chosen and further experiments were performed at fixed power and pressure. Figure 1 panels b–d show AFM images of BP flakes: as-exfoliated (Figure 1b), after 24 h of storage in low vacuum (10^{-1} Torr, Figure 1c), and after plasma treatment for 4 min (Figure 1d). The thicknesses of the as-exfoliated BP films vary in the range 4–50 nm, as found for the regions ①–⑤ in Figures 1b–d. Even after brief exposure to the atmosphere, a formation consisting of uniformly distributed protuberances or defects is evident on the top surface of the as-exfoliated BP film, as shown in Figure 1b. These protuberances appear to have grown from the top surface of the BP film rather than the edges. The AFM image in Figure 1c shows the same BP sample after storage for 24 h at 10^{-1} Torr. The surface degradation has intensified, merging into wider and taller bubbles with decreased density. Similar results have recently been reported for BP flakes.[17−22] The degradation of the BP surface after storage for 24 h also manifests in an increase in the surface roughness RMS value from 2.8 nm (as-exfoliated) to 4.7 nm. This chemical instability of BP is probably related to the electrostatics and structural buckling of its surface,[22] and has a serious negative impact on the performances of electronic devices, as discussed below. However, a subsequent plasma treatment (Ar+, 350 W, 4 min) of the same BP sample was found to completely remove the bubbles from the BP top surface, as shown in Figure 1d, producing a clean surface with a reduced surface RMS of less than 1 nm. The AFM height profiles were measured from the red boxes marked in Figure 1b–d. The line profiles in Figures 1b–d clearly show surface roughness and thickness change after the plasma treatments. Another important effect of the plasma treatment is a uniform decrease in the BP layer thickness. As shown in Figure 1e, the BP thicknesses in the regions marked ①–⑤ of the as-exfoliated sample (Figure 1b) decrease by ~6 nm after plasma treatment for 4 min (Figure 1d). The decrease in the thickness after 24 h of storage is due to the conversion of the top BP layer to the phosphorus oxide compounds, which introduces significant roughness onto the top surface. Figure S1 shows the degradation of the surface morphology and the decreases in the Raman peak intensities as the BP exposure time increases. We further determined the variation with plasma treatment duration in the BP thickness, that is, the decreases in thickness with increases in the plasma treatment period, as shown in Figure 1f. This figure shows that by adjusting the plasma treatment duration, the BP thickness can be controlled in a monotonic manner. Figure 1g shows the Raman spectra of the BP samples with thicknesses ranging from 2 to 10 nm, which were obtained by varying the plasma treatment duration. In these spectra there are three prominent peaks at 366 cm^{-1}, 443 cm^{-1}, and 471 cm^{-1}. The spectra are normalized to the Raman peak of the A^2_g peak at 471 cm^{-1}. These peaks are due to vibrations of the crystalline lattice of BP and match the Raman shifts attributed to the A^1_g, B_{2g}, and A^2_g phonon modes observed in bulk and exfoliated BP,[9,25,26] which indicates that the BP films retain their crystalline structures after plasma treatment, as also confirmed by the TEM analysis presented below. The vibration directions of the phosphorus atoms in the B_{2g} and A^2_g modes correspond to vibrational modes in which the atoms oscillate within the layer plane; in the A^1_g mode the phosphorus atoms vibrate out-of-plane.[9,26] While there is no significant variation with thickness in the Raman peaks of our BP films, the ratio of the intensities of the A^1_g peak and the Si peak monotonically increases from 0.02 to 1.69 as the BP thickness increases from 2 to 10 nm (Figure S2), which suggests that this ratio can be used as a gauge of BP film thickness.[9,25]

Further investigation of the surface morphologies of the BP films was performed with SEM analysis. Figure 2a–c show SEM images of BP films prepared under identical conditions (thickness: 10–20 nm) to the BP films in Figure 1b–d. Shortly after exposure to the ambient atmosphere, small topographic protuberances are evident on the BP surface (Figure 2a). After 24 h of exposure, they have merged to form larger bubbles (Figure 2b). However, after plasma treatment for 4 min, the impurities formed on top of the BP surface have been successfully removed (Figure 2c). These results indicate that the optimized plasma treatment etches the BP flake layer-by-layer so that the remaining layers retain good morphology and a clean chemical structure. To check for chemical modifications and the formation of additional chemical bonds on the BP surface, XPS was performed. Figure 2d displays the P 2p core XPS spectra of the as-exfoliated BP flakes (thickness: 10–20 nm) after 20 min of exposure (black curve), after 3 days of ambient exposure (red curve), and after 4 min of plasma treatment (blue curve). All spectra were calibrated to the binding energy of adventitious carbon (284.8 eV), and we compensated for electrostatic charging by using an Ar+ flood gun. The as-exfoliated BP produces a single spin–orbit split doublet at ~130 eV, which is consistent with previous XPS measurements for BP bulk crystals,[27,28] and there is an additional broad peak at ~135 eV. This feature is due to phosphate species, as many oxidized phosphorus compounds exhibit peaks near 134–136 eV.[22,27] Wide oxidized phosphorus peaks suggest oxide amorphization, with multiple P–O and P═O bonding states. Therefore, we assign the peaks to POx, that is, oxidized phosphorus species. The intensity of the broad POx peak is comparatively weak because of the short time exposure and incomplete oxidation

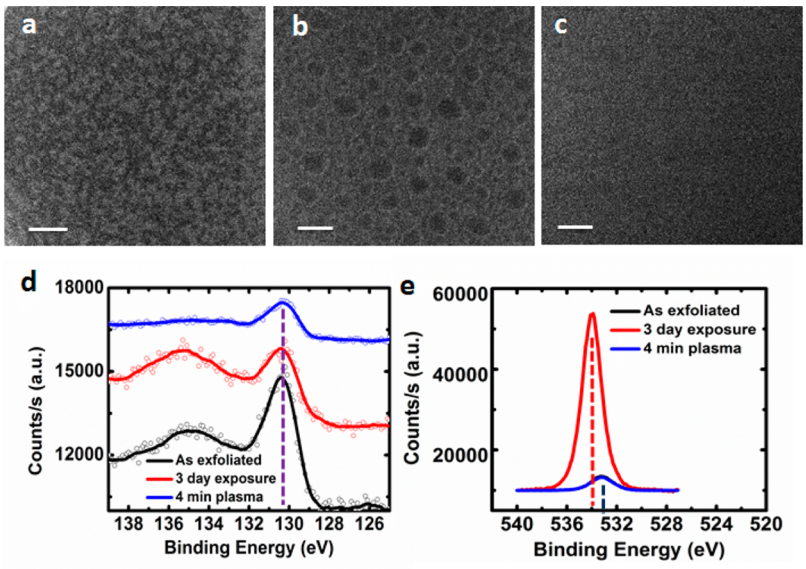

Figure 2. (a–c) SEM images of BP samples prepared under the same conditions as in Figures 1(b–d). Scale bars are 100 nm. XPS spectra of the (d) P 2p and (e) O 1s cores of the BP samples in panels a–c.

reaction. After 3 days of ambient exposure, the intensity of the P 2p spectra of BP decreases, which is characteristic of increased oxidation that transforms phosphorus from the elemental form into a compound. Further oxidization results in POx spectra with higher intensity. After 4 min of plasma treatment, the significant decrease in the intensity of POx and similar P 2p peak is observed, which confirms that the plasma treatment not only has a thinning effect but also a cleaning function. Figure 2e shows the O 1s core XPS spectra of the same samples. The same peak is present at ~533 eV for both the as-exfoliated (black curve) and the plasma-treated samples (blue curve). The sharp peak at ~534 eV for the sample after 3 days exposure (red curve) also indicates that POx formation occurs on the BP surface after exposure to the ambient atmosphere, which is removed by the plasma treatment.

We employed TEM to further characterize the atomic structures and crystallinity of the as-exfoliated and plasma-treated as-exfoliated BP samples. Figure 3 panels a and c show high resolution TEM images of the as-exfoliated (~50 nm) and plasma-treated (~5 nm) BP films. Perfect and orderly atomic arrangements without noticeable defects are evident for both samples. Top view hexagonal structures are drawn on each image (red ball-and-stick). The estimated lattice constants are a = 2.13 Å, b = 1.33 Å, and c = 3.226 Å, which are consistent with the theoretical values and show that the ideal atomic structure and crystallinity persist during the plasma treatment.[6,9] Figure 3 panels b and d show the SAED (selective area energy diffraction) images corresponding to Figure 3 panels a and c. Single crystal structures are evident for both samples. The density of bright spots is higher in the SAED image of the plasma-treated sample (Figure 4d), and the (101) crystal orientation is prominent. The prominence of this orientation is due to the thinning of the BP sample by the plasma treatment, which enhances the light luminance of the (101) crystal orientation.[9]

Back-gated FETs were fabricated on Si substrates covered with thermally grown 285 nm SiO_2 layers, as shown in Figure 1a. Figures 4 panels a–c show OM images of FETs incorporating BP films with various thicknesses, which were obtained by applying plasma treatment to the same sample: as-exfoliated BP (~30 nm), after 8 min of plasma treatment (~18 nm), and after 13 min of plasma treatment (~10 nm). After characterizing the as-exfoliated BP FET, plasma treatments were applied to the BP channel for 8 and 5 min to reduce the thickness. Figure 4d shows the I_d–V_g characteristics (V_{ds} = 100 mV) of the resulting films, which exhibit p-type dominant behaviors. A similar result was reported from the experimental work,[10] which is consistent with theoretical predictions.[13,29] However, the ambipolar conductions were also reported.[4,30,31] Further thorough investigations are required to clarify this. As the duration of the plasma treatment period increases, that is, the BP thickness decreases, enhanced transfer characteristics are obtained: the mobility increases from 70 $cm^2 V^{-1} s^{-1}$ (as-exfoliated) to 160 $cm^2 V^{-1} s^{-1}$ (8 min of plasma treatment) and 415 $cm^2 V^{-1} s^{-1}$ (13 min of plasma treatment), the on–off ratio increases and hysteresis decreases (Figure S7). These improvements can be attributed to the combined effects of the reduction in thickness and the defect removal by the plasma treatment. The contact between the metal electrodes and the BP layers exhibited ohmic contact behavior, as confirmed by the linear I_d–V_d curves with various V_g (Figure S11). Here, the field-effect carrier mobility was extracted from the equation $\mu = d\sigma/(C_g \cdot dV_g) = (L/C_g W V_{ds}) \cdot (dI_{ds}/dV_g)$, where μ is the field-effect mobility, L and W are the channel length and width, respectively,

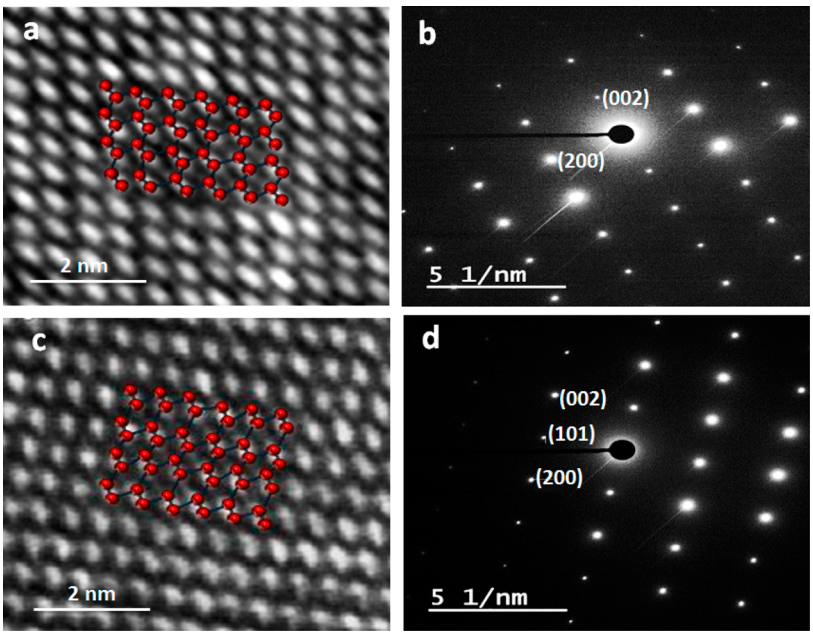

Figure 3. (a) TEM image and (b) SAED pattern for the as-exfoliated BP sample, and (c) TEM image and (d) SAED pattern for the plasma-treated BP sample.

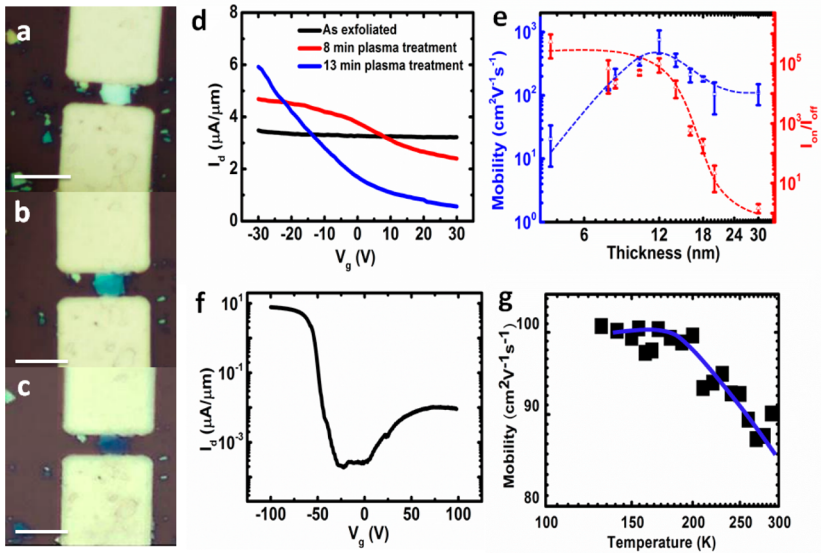

Figure 4. (a–c) OM images of the fabricated back-gated FETs incorporating the following BP films: as-exfoliated, after 8 min of plasma treatment, and after 13 min of plasma treatment, respectively. Scale bars are 10 μm. (d) I_d–V_g transfer characteristics of the three FETs; (e) the I_{on}/I_{off} ratio and field-effect mobility as functions of BP film thickness; (f) I_d–V_g transfer characteristics of the 12 nm thickness BP FET which exhibits the highest mobility; (g) the temperature dependence of the field-effect mobility.

C_g is the gate capacitance of the SiO_2 dielectric, and I_{ds} is the drain current. The variations with thickness in the field-effect mobility and the I_{on}/I_{off} ratio were investigated by preparing BP films with various thicknesses by applying plasma treatment for different periods. A four-terminal measurement was also conducted on the fabricated BP FETs. A similar mobility value was obtained, as shown in Figure S12. The variation with thickness in the field-effect mobilities of the BP FETs (Figure 4e) exhibits a characteristic behavior found for other layered materials,[32,33] which is due to two mechanisms: the carrier scattering induced by charge impurities at the interface between the BP channel and the SiO_2 substrate and the increases in the interlayer resistance with increases in the layer thickness. A thinner BP channel is more susceptible to potential variations in the substrate due to the formation of traps at the interface. The mobility increases monotonically in the thickness range 4–12 nm because charge screening by induced charge is enhanced as the BP film thickness increases. However, further increases in channel thickness will result in increases in the interlayer resistance of the BP

films, and thus in decreases in carrier conduction from the electrical contacts formed on the top surfaces of the BP films. The degradation of the I_{on}/I_{off} ratio could be also related to the incomplete removal of the defects on the BP surface. A peak mobility of 1150 $cm^2 V^{-1} s^{-1}$ was obtained at a BP thickness of ~12 nm (I_d-V_g characteristics of this device is shown in Figure 4f). Although this result is lower than the theoretically predicted mobility (20000 $cm^2 V^{-1} s^{-1}$)[9] and the recently reported mobility from the h-BN/BP/h-BN stacked structure,[34] it is the highest BP FET mobility observed so far fabricated on SiO_2 substrate at room temperature.

Recent experimental studies have shown that chemical instability in the BP surface results in the degradation of BP FET performance.[20−22] The stabilities of the FETs with plasma-treated BP films fabricated in this study are shown in Figure S3. The as-fabricated FET with a plasma-treated BP film (~8 nm) yields an initial I_{on}/I_{off} ratio ~10^3 with a field-effect mobility of 100 $cm^2 V^{-1} s^{-1}$. However, after 5 h of ambient exposure, the on current decreased by a factor of ~10 and the threshold voltage shifted to ~50 V, which is due to the formation of PO_x species on the top surface and p-type doping by the adsorbates. Further exposures of 20 and 40 h were found to result in the complete degradation of the transfer characteristics, as shown in Figure S3a. To overcome this problem, some works have been reported such as PMMA, ALD grown Al_2O_3, and h-BN encapsulation.[18,22,34,35] In our work, the PMMA-passivation was used to protect the prepared BP films from water and oxygen molecules in air. As shown in Figure S4, the PMMA-passivated BP film (~8 nm) maintains its good morphology and surface roughness even after a long exposure to air, and exhibits excellent Raman spectra. Further, this passivation capability is confirmed by the OM and AFM images taken after 15 days exposure as shown in Figure S5. A BP FET prepared identically to that shown in Figure S3a was passivated with a ~ 300 nm thick film of spin-coated PMMA immediately after fabrication and plasma treatment. The passivated device exhibits an initial hole mobility of 150 $cm^2 V^{-1} s^{-1}$ and an I_{on}/I_{off} ratio of 10^4. More importantly, it maintains excellent I_d-V_g transfer characteristics over several weeks (Figure S3b), that is, excellent environmental stability. The temperature dependence of the carrier mobilities of the BP FETs is shown in Figure 4g. Note that the carrier mobility saturates at low temperature and decreases when the temperature is increased from 170 to 300 K. The decay of the mobility in this temperature range follows a power law, $\mu \approx T^{-\gamma}$ with γ = 0.4. This exponent of the power law dependence is much lower than the theoretically predicted value of γ = 2.6 for a semiconducting layered structure.[36] This exponent of the power law dependence is slightly lower than the reported value of γ = 0.5 for a BP FET which has similar device structure.[10,37,38] The real cause of these discrepancies is not clear at this moment; further thorough theoretical and experimental studies are needed for complete understanding of the mechanism of carrier transport in BP FETs.

CONCLUSION

We have demonstrated that the thickness of exfoliated BP films can be controlled by performing an optimized plasma etching process on the top surface of the BP film. Our AFM, SEM, and TEM results showed that the plasma treatment successfully removes the POx species formed on the BP surface and that the remaining few-layer BP films exhibit excellent morphology and crystalline structure. The chemical instability of the exposed BP film was resolved by passivation with PMMA. The plasma-treated thickness-controlled BP films and their passivation with PMMA were used to fabricate an FET with a high field-effect mobility of 1150 $cm^2/(V s)$, an I_{on}/I_{off} ratio of ~10^5 at room temperature, and excellent environmental stability.

EXPERIMENTAL SECTION

Materials and Methods. Few-layer BP was obtained by cleaving commercially available bulk BP crystals with blue Nitto tape. After exfoliation, for further thickness control, an inductively coupled plasma (ICP) was used to treat the BP flakes. Ar gas was used to maintain the pressure at 30 mTorr, and 350 W rf power delivered at 13.56 MHz was applied to a four-turn spiral coil to discharge the high density plasma. For the passivation of the BP film, we directly coated it after plasma treatment with PMMA (495, A5) by using a spin coater with a rotation speed of 5000 rpm for 50 s.

Characterization. The surface morphologies of the samples were examined with AFM (Veeco Icon) and SEM (JEOL JSM-7401F). AFM images were acquired in air cantilevers operated in tapping mode. Raman spectroscopy was performed with a laser micro-Raman spectrometer (Kaiser Optical Systems RAMANRXN1, at an excitation wavelength of 532 nm). For the TEM (JEOL JEM 2100F) measurements, the BP samples were transferred onto a copper grid with carbon mesh. TEM imaging was carried out at an acceleration voltage of 300 kV. The chemical configurations were determined with X-ray photoelectron spectroscopy (XPS, ESCA2000). The XPS measurements were performed with an Al Kα and Mg Kα X-ray source. The spot sizes of the XPS measurements are 1 cm.

FET Fabrication. For the fabrication of the plasma-treated BP FETs, we first exfoliated BP onto a SiO_2 substrate, followed by ~10 min of plasma treatment to produce thinner BP flakes. After the plasma treatment, we directly coated PMMA onto the films. OM was used to find a BP flake with a thickness of <20 nm and a suitable size, then electron-beam lithography was used to fabricate back-gated FETs and Cr/Pd (5 nm/50 nm) was deposited with an e-beam evaporator, followed by a lift off process. Then we again applied plasma treatment to the BP FET to prepare a BP film with the required thickness by controlling the treatment duration and removing the oxides at the same time. Finally, PMMA was coated onto the BP film right after the plasma treatment so as to isolate the BP FET from the ambient atmosphere. The fabricated back-gated transistors

were characterized by using a Keithley 4200 parameter analyzer at the pressure of 10^{-2} Torr.

Conflict of Interest: The authors declare no competing financial interest.

Acknowledgment. This research was supported by the Global Frontier Program through the Global Frontier Hybrid Interface Materials (GFHIM) (2013M3A6B1078873) of the National Research Foundation of Korea (NRF) and the Pioneer Research Center Program through the National Research Foundation of Korea funded by the Ministry of Science, ICT & Future Planning (2014M3C1A3053024), and Basic Science Research Program through the National Research Foundation of Korea funded by the Ministry of Science, ICT & Future Planning (Grant No. 2009-0083540 and Grant No. 2012R1A1A2020089).

Supporting Information Available: The Supporting Information is available free of charge on the ACS Publications website at DOI: 10.1021/acsnano.5b04265.

Time dependence of the degradation of an exfoliated BP film on SiO_2 substrate; thickness dependence of the ratio of the intensities of the A^1_g and Si Raman peaks; environmental stability with PMMA passivation, hysteresis, I_d-V_g, I_d-V_d characteristic and four-probe measurement of the thin BP FETs; plasma process optimization for controlled etching of the BP film (PDF)

REFERENCES AND NOTES

1. Geim, A. K. Graphene: Status and Prospects. *Science* **2009**, *324*, 1530–1534.
2. Xu, J.; Jang, S. K.; Lee, J.; Song, Y. J.; Lee, S. The Preparation of BN-Doped Atomic Layer Graphene *via* Plasma Treatment and Thermal Annealing. *J. Phys. Chem. C* **2014**, *118*, 22268–22273.
3. Churchill, H. O.; Jarillo-Herrero, P. Two-Dimensional Crystals: Phosphorus Joins the Family. *Nat. Nanotechnol.* **2014**, *9*, 330–331.
4. Koenig, S. P.; Doganov, R. A.; Schmidt, H.; Neto, A. C.; Oezyilmaz, B. Electric Field Effect in Ultrathin Black Phosphorus. *Appl. Phys. Lett.* **2014**, *104*, 103106.
5. Wang, Q. H.; Kalantar-Zadeh, K.; Kis, A.; Coleman, J. N.; Strano, M. S. Electronics and Optoelectronics of Two-Dimensional Transition Metal Dichalcogenides. *Nat. Nanotechnol.* **2012**, *7*, 699–712.
6. Hultgren, R.; Gingrich, N.; Warren, B. The Atomic Distribution in Red and Black Phosphorus and the Crystal Structure of Black Phosphorus. *J. Chem. Phys.* **1935**, *3*, 351–355.
7. Stephenson, C.; Potter, R.; Maple, T.; Morrow, J. The Thermodynamic Properties of Elementary Phosphorus The Heat Capacities of Two Crystalline Modifications of Red Phosphorus, of α and β White Phosphorus, and of Black Phosphorus from 15 to 300 K. *J. Chem. Thermodyn.* **1969**, *1*, 59–76.
8. Appalakondaiah, S.; Vaitheeswaran, G.; Lebegue, S.; Christensen, N. E.; Svane, A. Effect of van der Waals Interactions on the Structural and Elastic Properties of Black Phosphorus. *Phys. Rev. B: Condens. Matter Mater. Phys.* **2012**, *86*, 035105.
9. Castellanos-Gomez, A.; Vicarelli, L.; Prada, E.; Island, J. O.; Narasimha-Acharya, K.; Blanter, S. I.; Groenendijk, D. J.; Buscema, M.; Steele, G. A.; Alvarez, J. Isolation and Characterization of Few-Layer Black Phosphorus. *2D Mater.* **2014**, *1*, 025001.
10. Li, L.; Yu, Y.; Ye, G. J.; Ge, Q.; Ou, X.; Wu, H.; Feng, D.; Chen, X. H.; Zhang, Y. Black Phosphorus Field-Effect Transistors. *Nat. Nanotechnol.* **2014**, *9*, 372–377.
11. Liu, H.; Du, Y.; Deng, Y.; Ye, P. D. Semiconducting Black Phosphorus: Synthesis, Transport Properties and Electronic Applications. *Chem. Soc. Rev.* **2015**, *44*, 2732–2743.
12. Zhang, S.; Yang, J.; Xu, R.; Wang, F.; Li, W.; Ghufran, M.; Zhang, Y.-W.; Yu, Z.; Zhang, G.; Qin, Q. Extraordinary Photoluminescence and Strong Temperature/Angle-Dependent Raman Responses in Few-Layer Phosphorene. *ACS Nano* **2014**, *8*, 9590–9596.
13. Qiao, J.; Kong, X.; Hu, Z.-X.; Yang, F.; Ji, W. High-Mobility Transport Anisotropy and Linear Dichroism in Few-Layer Black Phosphorus. *Nat. Commun.* **2014**, *5*, 4475.
14. Rudenko, A. N.; Katsnelson, M. I. Quasiparticle Band Structure and Tight-Binding Model for Single-and Bilayer Black Phosphorus. *Phys. Rev. B: Condens. Matter Mater. Phys.* **2014**, *89*, 201408.
15. Chang, K.; Cohen, M. L. Structural Stability of Phases of Black Phosphorus. *Phys. Rev. B: Condens. Matter Mater. Phys.* **1986**, *33*, 6177.
16. Sugai, S.; Ueda, T.; Murase, K. Pressure Dependence of the Lattice Vibration in the Orthorhombic and Rhombohedral Structures of Black Phosphorus. *J. Phys. Soc. Jpn.* **1981**, *50*, 3356–3361.
17. Avsar, A.; Vera-Marun, I. J.; Tan, J. Y.; Watanabe, K.; Taniguchi, T.; Castro Neto, A. H.; Özyilmaz, B. Air-Stable Transport in Graphene-Contacted, Fully Encapsulated Ultrathin Black Phosphorus-Based Field-Effect Transistors. *ACS Nano* **2015**, *9*, 4138–4145.
18. Doganov, R. A.; O'Farrell, E. C.; Koenig, S. P.; Yeo, Y.; Ziletti, A.; Carvalho, A.; Campbell, D. K.; Coker, D. F.; Watanabe, K.; Taniguchi, T. Transport Properties of Pristine Few-Layer Black Phosphorus by van der Waals Passivation in An Inert Atmosphere. *Nat. Commun.* **2015**, *6*, 6647.
19. Favron, A.; Gaufrès, E.; Fossard, F.; Phaneuf-L'Heureux, A.-L.; Tang, N. Y.; Lévesque, P. L.; Loiseau, A.; Leonelli, R.; Francoeur, S.; Martel, R. Photooxidation and Quantum Confinement Effects in Exfoliated Black Phosphorus. *Nat. Mater.* **2015**, *14*, 826–832.
20. Island, J. O.; Steele, G. A.; van der Zant, H. S.; Castellanos-Gomez, A. Environmental Instability of Few-Layer Black Phosphorus. *2D Mater.* **2015**, *2*, 011002.
21. Kim, J.-S.; Liu, Y.; Zhu, W.; Kim, S.; Wu, D.; Tao, L.; Dodabalapur, A.; Lai, K.; Akinwande, D. Toward Air-Stable Multilayer Phosphorene Thin-Films and Transistors. *Sci. Rep.* **2015**, *5*, 8989.
22. Wood, J. D.; Wells, S. A.; Jariwala, D.; Chen, K.-S.; Cho, E.; Sangwan, V. K.; Liu, X.; Lauhon, L. J.; Marks, T. J.; Hersam, M. C. Effective Passivation of Exfoliated Black Phosphorus Transistors Against Ambient Degradation. *Nano Lett.* **2014**, *14*, 6964–6970.
23. Ziletti, A.; Carvalho, A.; Campbell, D.; Coker, D.; Neto, A. C. Oxygen Defects in Phosphorene. *Phys. Rev. Lett.* **2015**, *114*, 046801.
24. Ziletti, A.; Carvalho, A.; Trevisanutto, P.; Campbell, D.; Coker, D.; Neto, A. C. Phosphorene Oxides: Bandgap Engineering of Phosphorene by Oxidation. *Phys. Rev. B: Condens. Matter Mater. Phys.* **2015**, *91*, 085407.
25. Lu, W. L.; Nan, H. Y.; Hong, J. H.; Chen, Y. M.; Zhu, C.; Liang, Z.; Ma, X. Y.; Ni, Z. H.; Jin, C. H.; Zhang, Z. Plasma-Assisted Fabrication of Monolayer Phosphorene and Its Raman Characterization. *Nano Res.* **2014**, *7*, 853–859.
26. Sugai, S.; Shirotani, I. Raman and Infrared Reflection Spectroscopy in Black Phosphorus. *Solid State Commun.* **1985**, *53*, 753–755.
27. Brunner, J.; Thüler, M.; Veprek, S.; Wild, R. X-ray Photoelectron Study of Amorphous Phosphorus Prepared by Plasma Chemical Transport. Comparison with Crystalline Polymorphs. *J. Phys. Chem. Solids* **1979**, *40*, 967–971.
28. Harada, Y.; Murano, K.; Shirotani, I.; Takahashi, T.; Maruyama, Y. Electronic Structure of Black Phosphorus Studied by X-Ray Photoelectron Spectroscopy. *Solid State Commun.* **1982**, *44*, 877–879.
29. Morita, A. Semiconducting Black Phosphorus. *Appl. Phys. A: Solids Surf.* **1986**, *39*, 227–242.
30. Das, S.; Demarteau, M.; Roelofs, A. Ambipolar Phosphorene Field Effect Transistor. *ACS Nano* **2014**, *8*, 11730–11738.
31. Zhu, W.; Yogeesh, M. N.; Yang, S.; Aldave, S. H.; Kim, J.-S.; Sonde, S.; Tao, L.; Lu, N.; Akinwande, D. Flexible Black Phosphorus Ambipolar Transistors, Circuits and AM Demodulator. *Nano Lett.* **2015**, *15*, 1883–1890.
32. Bao, W.; Cai, X.; Kim, D.; Sridhara, K.; Fuhrer, M. S. High Mobility Ambipolar MoS2 Field-Effect Transistors: Substrate and Dielectric Effects. *Appl. Phys. Lett.* **2013**, *102*, 042104.

33. Das, S.; Chen, H.-Y.; Penumatcha, A. V.; Appenzeller, J. High Performance Multilayer MoS2 Transistors with Scandium Contacts. *Nano Lett.* **2012**, *13*, 100–105.
34. Chen, X.; Wu, Y.; Wu, Z.; Xu, S.; Wang, L.; Han, Y.; Ye, W.; Han, T.; He, Y.; Cai, Y. High Quality Sandwiched Black Phosphorus Heterostructure and Its Quantum Oscillations. *Nat. Commun.* **2015**, *6*, 7315.
35. Tayari, V.; Hemsworth, N.; Fakih, I.; Favron, A.; Gaufrès, E.; Gervais, G.; Martel, R.; Szkopek, T. Two-Dimensional Magnetotransport in a Black Phosphorus Naked Quantum Well. *Nat. Commun.* **2015**, *6*, 7702.
36. Fivaz, R.; Mooser, E. Mobility of Charge Carriers in Semiconducting Layer Structures. *Phys. Rev.* **1967**, *163*, 743.
37. Ong, Z.-Y.; Zhang, G.; Zhang, Y. W. Anisotropic Charged limpurity-Limited Carrier Mobility in Monolayer Phosphorene. *J. Appl. Phys.* **2014**, *116*, 214505.
38. Xia, F.; Wang, H.; Jia, Y. Rediscovering Black Phosphorus as an Anisotropic Layered Material for Optoelectronics and Electronics. *Nat. Commun.* **2014**, *5*, 4458.